Journal of Enzyme Inhibition and Medicinal Chemistry, April 2009; 24(2): 471–479

Particular interaction between pyrimethamine derivatives and quadruple mutant type dihydrofolate reductase of *Plasmodium falciparum*: CoMFA and quantum chemical calculations studies

PHORNPHIMON MAITARAD[1,2], PATCHREENART SAPARPAKORN[1,2], SUPA HANNONGBUA[1,2], SUMALEE KAMCHONWONGPAISAN[3], BONGKOCH TARNCHOMPOO[3], & YONGYUTH YUTHAVONG[3]

[1]*Department of Chemistry, Faculty of Science, Kasetsart University, Bangkok 10900, Thailand,* [2]*Center of Nanotechnology KU, Kasetsart University and NANOTEC Center of Excellence at Kasetsart University, Pathumthani 12120, Thailand, and* [3]*National Center for Genetic Engineering and Biotechnology, National Science and Technology Development Agency, Pathumthani 12120, Thailand*

(*Received 26 September 2007; revised 6 February 2008; accepted 25 February 2008*)

Abstract

Comparative molecular field analysis (CoMFA) was performed on twenty-three pyrimethamine (pyr) derivatives active against quadruple mutant type (Asn51Ile, Cys59Arg, Ser108Asn, Ile164Leu) dihydrofolate reductase of *Plasmodium falcipaarum* (*Pf*DHFR). The represented CoMFA models were evaluated based on the various three different probe atoms, C_{sp3} (+1), O_{sp3} (−1) and H (+1), resulting in the best model with combined three types of probe atoms. The statistical results were $r^2_{cv} = 0.702$, $S_{press} = 0.608$, $r^2_{nv} = 0.980$, s = 0.156, and $r^2_{test-set} = 0.698$ which can explain steric contribution of about 50%. In addition, an understanding of particular interaction energy between inhibitor and surrounding residues in the binding pocket was performed by using MP2/6-31G(d,p) quantum chemical calculations. The obtained results clearly demonstrate that Asn108 is the cause of pyr resistance with the highest repulsive interaction energy. Therefore, CoMFA and particular interaction energy analyses can be useful for identifying the structural features of potent pyr derivatives active against quadruple mutant type *Pf*DHFR.

Keywords: *Dihydrofolate reductae, pyrimethamine, CoMFA, quantum chemical calculations*

Introduction

Malaria is one of the most common infectious diseases and an enormous public-health problem which kills approximately 400 million people every year, especially in tropical and subtropical regions [1]. The disease is caused by protozoan parasites of the genus *Plasmodium*. The most serious form of the disease is caused by *Plasmodium falciparum* (*Pf*). Dihydrofolate reductase (DHFR) of *Pf* is an important target for malaria chemotherapy. In malaria, DHFR is a bifunctional enzyme with Thymidilate synthase (TS), which is known to be essential for DNA synthesis [2–4]. Inhibition of DNA synthesis through inhibition of *Pf*DHFR can be done by preventing dihydrofolate to forming tetrahydrofolate by using an antifolate such as pyrimethamine (pyr) and cycloguanil drugs. Pyr is an effective, sentitive and selective antifolate drug against the wild type *Pf*DHFR but its antimalarial action is slow [5]. Generally, pyr is used in combinations with other antifolates, such as Maloprim (pyr-dapsone) [6] and Fansidar (pyr-sulfadoxine) [7,8].

Unfortunately, resistance to antifolates has been found after using them as antimalarial drugs. It has been reported that antifolate drug resistance is due to

Correspondence: S. Hannongbua, Department of Chemistry, Kasetsart University, Bangkok 10900, Thailand. Fax: 66 25 62 55 55 Ext. 2140. E-mail: fscisph@ku.ac.th

ISSN 1475-6366 print/ISSN 1475-6374 online © 2009 Informa UK Ltd.
DOI: 10.1080/14756360802201223

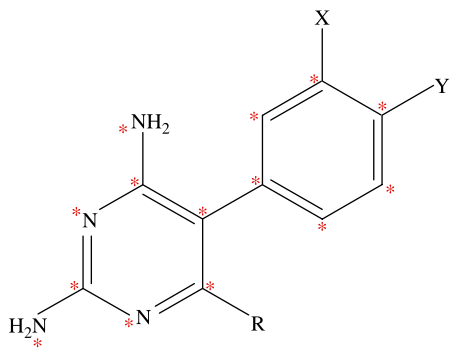

Figure 1. Template structure of 5-phenyl-2,4-diamonopyrimidine derivatives.

point mutations in *Pf*DHFR. The most important one is Ser108 to Asn108 mutation in the active site of *Pf*DHFR. Additional point mutations in Asn51Ile, Cys59Arg and Ile164Leu were associated with higher levels of resistance to the conventional antifolate drugs [9–15].

In developing more potent pyr antimalarial derivatives against pyr-resistant parasites, Kamchonwongpaisan et al. [16] reported a series of pyr derivatives including the structural modification, synthesis, and biological assay of the *Pf*DHFR enzyme. Based on the structure of pyr modifications at position **X** and **Y** and **R** substitutions on 5-phenyl ring of the 2,4 diaminopyrimidine ring contribute to the improvement in its antimalarial activity, as shown in Figure 1. Both structures and biological activities, in terms of inhibition constant (K_i), of these pyr derivatives are shown in Table I. Following the discovery of these effective pyr derivatives, a 3D-QSAR (Three Dimentional-Quantitative Structure Activity Relationship) study of these compounds was carried out in order to investigate the local physicochemical properties involving in drug and receptor interactions. In this report, comparative molecular field analysis (CoMFA), one of the most useful tools for 3D-QSAR study [17–21], by relating the biological activity of a series of molecules with their steric and electrostatic fields was employed. CoMFA was performed on pyr derivatives to determine the structural requirements for improving binding to quadruple mutant type of *Pf*DHFRs (Asn51Ile, Cys59Arg, Ser108Asn, Ile164Leu). In addition, the particular interaction energy between an inhibitor and surrounding amino acids in the binding pocket of quadruple mutant *Pf*DHFR was also determined by quantum chemical calculations. Combination of the tools has led to investigation of inhibitor-enzyme interactions at the molecular level. Due to limitations of molecular systems by its complexity size [22,23], the analysis was therefore performed by limiting the interaction boundary to only 4 Å surrounding the ligand molecule in the active site of quadruple mutant *Pf*DHFR. Comparisons of the particular interaction energy were made between pyr and the potent derivative, compound **6**. Both the CoMFA method and quantum chemical calculations provide crucial information not only on the spatial orientation of the ligands and the main amino acid

Table I. Data set used for CoMFA analysis with K_i (nM) and pK_i values in the quadruple mutant (Asn51Ile, Cys59Arg, Ser108Asn, Ile164Leu) of *Pf*DHFR.

Cpd	**X**	**Y**	**R**	K_i (nM)	pK_i
1 (P1)	H	Cl	Et	385	6.41
2 (P15)[a]	-OCH_2O-		Et	269	6.57
3 (P17)	H	Me	Et	284	6.55
4 (P13)	Cl	Cl	Et	53	7.27
5 (P20)[a]	H	H	Et	32	7.49
6 (P30)	Cl	H	Et	3.3	8.48
7 (P16)	H	Cl	$(CH_2)_3COOMe$	360	6.44
8 (P26)	H	H	$(CH_2)_3COOMe$	24	7.62
9 (P29)[a]	Cl	H	$(CH_2)_3COOMe$	2.7	8.57
10 (P12)[a]	H	Cl	$(CH_2)_3Ph$	170	6.77
11 (P33)	H	H	$(CH_2)_3Ph$	4.7	8.33
12 (P31)	Cl	H	$(CH_2)_3Ph$	2	8.70
13 (P45)	H	H	$(CH_2)_3OH$	549	6.26
14 (P41)	Cl	H	$(CH_2)_3OH$	57	7.24
15 (P46)	H	H	$(CH_2)_3OCOCH_3$	237	6.62
16 (P42)	Cl	H	$(CH_2)_3OCOCH_3$	31.4	7.50
17 (P47)	H	H	$(CH_2)_3OCOC_6H_5$	14	7.85
18 (P43)	Cl	H	$(CH_2)_3OCOC_6H_5$	3.6	8.44
19 (P39)	H	H	nC_6H_{13}	1.4	8.85
20 (P44)	Cl	H	$(CH_2)_3OCOOCH_2C_6H_5$	3.6	8.44
21 (P38)	Cl	H	Me	14	7.85
22 (P32)	Cl	H	$(CH_2)_3C_6H_4$-(*p*-Ome)	2	8.70
23 (P40)[a]	Cl	H	$(CH_2)_2O(CH_2)_3OPh$	1.7	8.77

[a]Test set compounds

interactions but also on design of new potent inhibitors effective against the mutant *Pf*DHFR enzyme.

Methods

Biological data

Twenty-three pyr derivatives used for the CoMFA study were selected from Kamchonwongpaisan et al. [16] as shown in Table I. In this table, eighteen compounds served as the training set. In addition, five compounds that were selected from the diversity and ranges of biological activities were kept to evaluate the predictive power of the models as the test set. As the structure of the X and Y substituents of compound **2** are different from others due to the fused X-Y substitution, therefore, this compound was selected into the test set. For each set of biological data, the K_i (nM) was measured *in vitro* under the same experimental conditions. Consequently, *in vitro* antimalarial activities were converted into the corresponding pK_i ($-\log K_i$) values. These values were used as dependent variables in the CoMFA study.

Methods of CoMFA study

The CoMFA method is a ligand-based QSAR technique. In this study, the CoMFA method was employed by Sybyl (version 7.0, Tripos Inc.) installed on a Silicon Graphics Octane2 workstation at the National Electronics and Computer Technology Center of Thailand [24]. The structures of pyr derivatives were built using the SKETCH module in Sybyl. The skeleton and conformation of pyr (compound **1**) was extracted from the crystal structure of a pyr complex with double mutant *Pf*DHFR with PDB code 1J3J. The other molecules were built taking compound **1** as a template and changing their substituents. Then energy minimizations of all the generated structures were performed using the tripos force field and the Gasteiger Hückel charges were calculated [25].

CoMFA is a 3D-QSAR method that provides steric and electrostatic values from Lennard-Jones and Coulombic potentials equations, respectively. The 3D cubic lattices, with 2 Å grid spacing, were generated around the aligned compounds based on the molecular volume of the structure. The lattices were defined automatically, and were extended by 4.0 Å in all directions. All the generated structures were aligned in a 3D lattice based on atom superposition by aligning 5-phenyl-2,4-diamonopyrimidine as shown with the asterisk in Figure 1, In this investigation, three different atoms, sp^3 carbon atom with +1 charge, sp^3 oxygen atom with −1 charge and H atom with +1 charge, served as probe atoms. The probe atoms were placed at each lattice point and their interactions with the steric and electrostatic fields with each atom in the molecule were calculated with CoMFA standard scaling. The default value of 30 kcal/mol was used as the maximum electrostatic and steric energy cutoff. The CoMFA fields were scaled by CoMFA-STD method in Sybyl. Then, a partial least squares technique (PLS) was employed to derive a CoMFA model expressing the correlation between the steric and electrostatic properties and the biological activities [26,27]. The orthogonal latent variables were extracted by the NIPALS algorithm and subjected to full cross-validation with the Leave-One-Out method (LOO) [28,29]. In order to speed up the analysis and reduce the amount of noise, the minimum sigma value was set to 2.0 kcal/mol. The analyses were carried out with a maximum of six components, and using the number of components (noc) at which the difference in the r^2_{cv} value between components was less than 0.05.

Predictive ability

The predictive ability of the model derived from the training set is expressed by the predictive r^2_{cv} value. The r^2_{cv} value is defined as

$$r^2_{cv} = 1.0 - \frac{\text{PRESS}}{\text{SSY}} \tag{1}$$

where, SSY stands for the variance of the biological activities around the mean value, and PRESS is the prediction error sum of squares derived from LOO.

$$\text{PRESS} = \sum_y (y_{\text{pred}} - y_{\text{actual}})^2 \tag{2}$$

$$\text{SSY} = \sum_y (y_{\text{actual}} - y_{\text{mean}})^2 \tag{3}$$

The uncertainty of the prediction is defined as

$$S_{\text{PRESS}} = \sqrt{\frac{\text{PRESS}}{n - k - 1}} \tag{4}$$

where k is the number of variables in the model and n is the number of compounds used in the study [30].

Particular interaction energy

In order to investigate specific interaction of different potency of pyr derivatives in quadruple mutant DHFR, particular interaction was determined by quantum chemical calculations. According to comparison between double mutant complex with pyr (1J3J) and quadruple mutant complex with WR99210 (1J3K) structures superimposition, it was found that the binding sites are quite similar with RMS = 0.435 Å as shown in Figure 2. Due to there being no pyr/quadruple mutant DHFR available, therefore, in this study, we proposed pyr and quadruple mutant complex, based on atom superposition. Considering the graphical backbone superimpostion, it can be implied that WR99210 and pyr oriented in the same binding position, therefore, pyr can be adapted into the quadruple mutant type *Pf*DHFR to find the estimated particular interaction energy. The selected inhibitors were compounds **1** (pyr

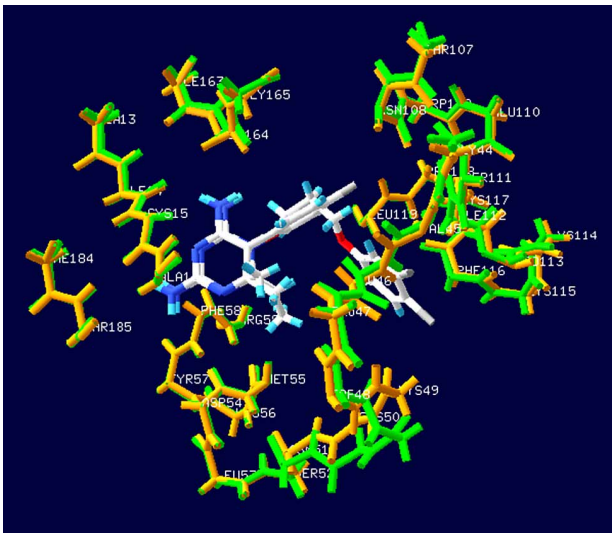

Figure 2. The backbone superimposition between the X-ray *Pf*DHFR/WR99210 complex structures of quadruple mutant (PDB entry 1J3K shown in green color) and *Pf*DHFR/pyr double mutant (PDB entry 1J3J shown in orange color), indicating the similarity binding position of both of the inhibitors.

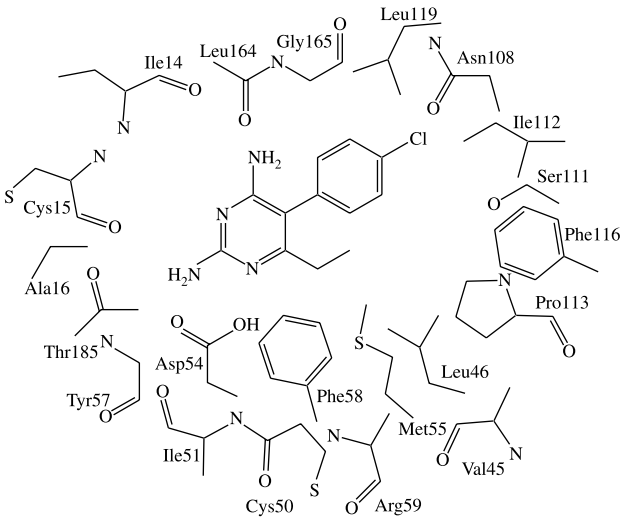

Figure 3. The 2D scheme of the adopted model system of inhibitor bound to the quadruple mutant type (Asn51Ile, Cys59Arg, Ser108Asn, Ile164Leu) of *Pf*DHFR binding site.

drug) and **6** according to their similar structures, but different K_i values. Compound **1** represented a resistance to quadruple mutant *Pf*DHFR while compound **6**, Cl substituent at **X**, gave a good K_i for this enzyme. The model systems contained compounds **1** or **6** and surrounding residues in the binding pocket with at least one atom interacting with any atoms of inhibitor within the interatomic distance of 4 Å that covered van der Waal interactions. The 22 selected residues were Ile14, Cys15, Ala16, Val45, Leu46, Trp48, Cys50, Ile51, Asp54, Met55, Tyr57, Phe58, Arg59, Asn108, Ser111, Ile112, Pro113, Phe116, Leu119, Leu164, Gly165 and Thr185. The four mutations, Asn51Ile, Cys59Arg, Ser108Asn and Ile164Leu, were also included in the system setup. The 2D scheme of the adopted model system of the inhibitor bound to the mutant *Pf*DHFR binding site is shown in Figure 3. In addition, the eleven inserted residues, 47, 49, 52, 53, 56, 109, 110, 114, 115, 117 and 118, were added into the system to complete the connection between the amino acids in the cutting chains. The N- and C-terminals were capped with a methyl amino group (-$NHCH_3$) and an acetyl group (CH_3CO-), respectively, which were retained from the backbone geometries of the nearby residues. Thus, the hydrogen atoms were added to the starting system using Sybyl7.0. Partial optimizations were performed by using the semiempirical PM3 method, implemented in the Gaussian 03 program [31], based on the 'heavy atoms fixing' approximation. Therefore, only H atoms of amino acids and all atoms of the inhibitor were optimized. Finally, MP2 calculations with 6-31G(d,p) basis set were applied to investigate the particular interaction energy between inhibitor and each residue surrounding the binding site as shown in the interaction energy formula:

$$E^{\mathrm{INT}}_{(\text{ligand}-\text{amino acid})} = E^{AB}_{(\text{ligand}-\text{amino acid})} - E^{A}_{(\text{ligand})} - E^{B}_{(\text{amino aicd})} \quad (5)$$

where A and B are the number of basis sets of ligands and amino acids, respectively, $E^{AB}_{(\text{ligand}-\text{amino acid})}$ is the energy of the ligand-amino acid complex with the basis set of A plus B. $E^{A}_{(\text{ligand})}$ and $E^{B}_{(\text{amino acid})}$ are the energies of ligand and amino acid with its number of basis sets. Moreover, the basis set superposition error based on counterpoise scheme (BSSE-CP) of Boys-Bernardi [32] was also computed to define the interaction energy with BSSE as shown in Equation 6:

$$E^{\mathrm{INT-BSSE}}_{(\text{ligand}-\text{amino acid})} = E^{AB}_{(\text{ligand}-\text{amino acid})} - E^{AB}_{(\text{ligand})} - E^{AB}_{(\text{amino aicd})} \quad (6)$$

where $E^{AB}_{(\text{ligand})}$ and $E^{AB}_{(\text{amino acid})}$ are the energies of ligand and amino acid, respectively, with the number of basis sets of A plus B [23].

Results and discussion

Statistical analysis

The relationship between structural properties of twenty-three pyr derivatives and their biological activities of quadruple mutant type *Pf*DHFR is presented by using the CoMFA model. There are three models that varied the type of probe atoms C_{sp3} (+1), O_{sp3} (−1) and H (+1) and the statistical results are shown in Table II. All models can be used to well predict the pK_i values for training compounds, with a residual not greater than 0.4; these results are summarized in Table III. Evaluation of the model

Table II. PLS statistical results of CoMFA models for quadruple mutant *Pf*DHFR.

	Probe Atoms			
Parameters	Model I C_{sp3} (+1)	Model II O_{sp3} (−1)	Model III H (+1)	Model IV C_{sp3} (+1), O_{sp3} (−1), H (+1)
no of molecules in training set	18	18	18	18
r^2_{cv}	0.724	0.669	0.690	0.702
S_{press}	0.560	0.641	0.620	0.608
no of components	5	6	6	6
r^2_{nv}	0.963	0.980	0.983	0.980
s	0.206	0.157	0.144	0.156
F value	62.152	90.708	108.191	92.183
Steric field contributions	0.613	0.567	0.519	0.547
Electrostatic field contributions	0.387	0.433	0.481	0.453
$r^2_{test-set}$	0.495	0.566	0.695	0.698

prediction is assessed by test set compounds which all showed acceptable pK_i prediction values, except compound **22**; this test set compound has a different structure of R substitution ($(CH_2)_2O(CH_2)_3OPh$) from the others, so it shows high residual pK_i between actual and predicted values.

By considering the statistical results in Table II, model I-III with r^2_{cv} values higher than 0.6 (0.724, 0.669 and 0.690, respectively) can be accepted and the conventional r^2 or no-validated r^2 (r^2_{nv}) values are found to be 0.963, 0.980 and 0.983, respectively. These mean that the three tested probes (Csp3, Osp3 and H) give qualitatively very similar models. The results suggest that all three types of probes form equally important in the enzyme-ligand interactions. Next, the combination of three probe atoms was used, resulting in model IV with $r^2_{cv} = 0.702$ and $r^2_{nv} = 0.980$. Moreover, the prediction for test set obtained from model IV shows the highest predictive ability ($r^2_{testset} = 0.698$). Therefore, the combining three probe atoms in model IV is superior and more general model. Especially, the statistical error (s) of the represented model is 0.156 which is reasonably acceptable for biological activity predictions of the training set and the test set. The graphical plot between actual and predicted pK_i of the training set and the test set is shown in Figure 4. The CoMFA field contributions of the steric and electrostatic interactions contributed approximately

Table III. Actual (Act) and predicted (Pred) pK_i values and the residuals (Δ) of the training set and test set molecules for the mutant *Pf*DHFR models.

		Pred	Δ	Pred	Δ	Pred	Δ	Pred	Δ
Cpd	Act	Model I		Model II		Model III		Model IV	
1	6.41	6.28	0.13	6.38	0.03	6.32	0.09	6.36	0.05
3	6.55	6.53	0.01	6.61	−0.07	6.61	−0.06	6.67	−0.13
4	7.27	7.58	−0.31	7.38	−0.10	7.31	−0.04	7.38	−0.10
6	8.48	8.12	0.36	8.16	0.32	8.24	0.23	8.16	0.32
7	6.44	6.54	−0.09	6.36	0.08	6.46	−0.01	6.35	0.09
8	7.62	7.50	0.11	7.77	−0.15	7.69	−0.07	7.77	−0.15
11	8.33	8.12	0.21	8.24	0.08	8.19	0.13	8.23	0.10
12	8.70	8.82	−0.12	8.79	−0.09	8.73	−0.04	8.79	−0.09
13	6.26	6.38	−0.12	6.44	−0.18	6.53	−0.27	6.45	−0.19
14	7.24	7.06	0.18	7.06	0.18	7.14	0.11	7.08	0.16
15	6.62	6.75	−0.13	6.60	0.02	6.51	0.11	6.57	0.06
16	7.50	7.38	0.12	7.40	0.10	7.41	0.09	7.44	0.06
17	7.85	7.91	−0.06	7.87	−0.02	7.85	−0.00	7.86	−0.01
18	8.44	8.45	−0.01	8.47	−0.02	8.52	−0.07	8.48	−0.04
19	8.85	8.78	0.07	8.86	−0.01	8.94	−0.09	8.89	−0.03
20	8.44	8.44	0.00	8.45	−0.01	8.42	0.02	8.44	0.01
21	7.85	8.15	−0.30	8.01	−0.16	7.95	−0.10	7.96	−0.11
22	8.70	8.77	−0.07	8.70	−0.00	8.74	−0.04	8.71	−0.01
2[a]	6.57	6.74	−0.17	6.76	−0.19	6.75	−0.18	6.75	−0.18
5[a]	7.49	6.89	0.60	7.28	0.21	7.31	0.18	7.26	0.23
9[a]	8.57	8.00	0.57	7.92	0.65	8.29	0.28	7.96	0.61
10[a]	6.77	7.63	−0.86	7.41	−0.64	7.38	−0.61	7.44	−0.67
23[a]	8.77	9.31	−0.54	9.81	−1.04	9.87	−1.10	9.65	−0.88

[a]Test set compounds

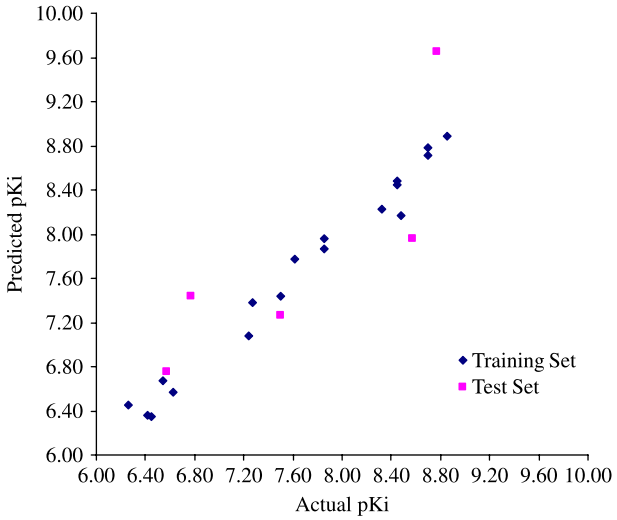

Figure 4. Plot of the predicted and actual pK_i values of the training set and the test set molecules with CoMFA H model IV.

50%. The results indicate that both steric and electrostatic contributions are equivalent that affected the biological activity of mutant *Pf*DHFR.

CoMFA contour analysis

The CoMFA analysis with hundreds or thousands terms, is usually represented as the scalar product of the associated coefficient and the standard deviation of all values in the corresponding column of the data table (STDEV*COEFF) contour plots. Moreover, the contour maps can be showed by merging with the binding pocket of a drug target. In this study, the CoMFA contour maps are merged with 7 Å of binding pocket of crystal structure of quadruple mutant type *Pf*DHFR which is available in the Protein Data Bank with PDB code 1J3K. The template compound **12** is displayed as the inhibitor in the CoMFA contour maps.

Figure 5 shows the steric contour maps of CoMFA model IV. The steric contour map indicates areas in which molecular steric bulk might have a favourable (green) or unfavourable (yellow) effect on the activity of an analogue. A sterically favoured green region is found near **X** substituent of the aromatic ring. This is further supported by comparing **X** substituent with Cl and H when these compounds have the same **Y** and **R** substituents. In addition, the distribution of steric contours appears around the phenyl side chain of **R** substituent; this evidence would explain why compound **12**, used as the template, is a better quadruple mutant *Pf*DHFR inhibitor than the pyr drug (compound **1**). Furthermore, this region is closed to Phe116 of the binding pocket. An unfavourable steric contour region is found at **Y** substituent on the aromatic ring which can explain the fact that compounds **1**, **7** and **10** show lower pK_i when compared with unsubstituted structures of compounds **5**, **8** and **11**, respectively.

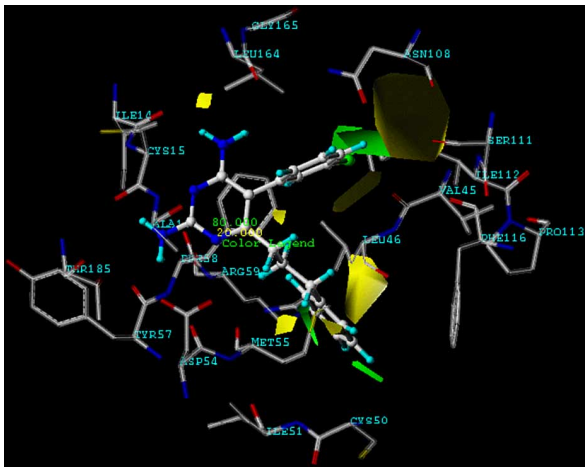

Figure 5. CoMFA (stdev.*coeff.) sterically favored areas are represented by green regions. Sterically unfavored areas are represented by yellow regions (level of steric contour contribution = 80%) and compound **12** is represented by ball and stick.

Therefore, a hydrogen atom is suitable substituent of **Y** position because the unfavourable steric area of **Y** is closed to an important mutation position, Asn108, of quadruple mutant *Pf*DHFR. The obtained unfavourable steric contour coincides with the previous publications [3,5,9,10] that reported a steric clash between the Cl substituent of pyr and the side chain of Asn108.

Figure 6 depicts electrostatic contour maps of CoMFA. The electrostatic contour map reveals that blue contours refer to positive charge favouring areas and red contours indicate negative charge favouring areas. The red area is found in the middle of the phenyl ring of **R** substitution which means high electron density in this area. Furthermore, a large blue contour also surrounds the phenyl ring of **R** substitution. It can

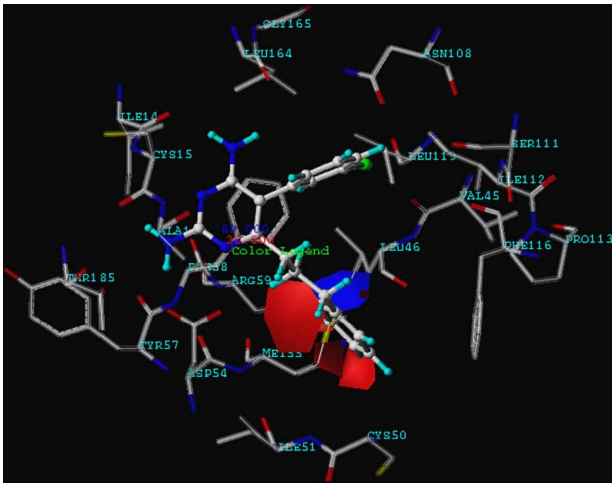

Figure 6. CoMFA (stdev.*coeff.) negative charge favored area is represented by the red region. Positive charge favored area is represented by the blue region (level of electrostatic contour contribution = 80%) and compound **12** is represented by ball and stick.

be suggested that high positive charges or low electron density in this area is preferable. Therefore, donating substituents of the phenyl ring will increase the activity of the inhibitors, for example, Cl, F, OCH_3, etc.

Particular interaction energy

In order to find the particular interaction energy between compound **1** or **6** and the amino acids surrounding the pocket of quadruple mutant type *Pf*DHFR, the MP2 method with basis set 6-31G(d,p) level of calculations was performed. In addition, the BSSE-CP was also calculated to correct the interaction energy. The obtained interaction energies are given in Table IV. Asp54 has the strongest interaction energy to compounds **1** and **6** of − 10.139 and − 10.250 kcal/mol, respectively. This amino acid formed H-bond interaction with the inhibitors. In addition, the H-bond interactions are also found with Ile14 and Leu164 for both compounds **1** and **6**. All H-bond distances are displayed in Figure 7. Three mutant amino acids, Ile51, Arg59 and Leu164, show no significantly different interaction energies between compound **1** and **6** (Table IV). While Asn108 shows more repulsive interaction to compound **1** by approximately 5 kcal/mol because compound **1** has the Cl substituent at **Y** position which can occur due to the steric clash with the side chain of Asn108, as shown clearly by electrostatic potential surfaces in Figure 8. In pervious reviews [33–35], there were many reports that proposed the cause of pyr resistance in quadruple mutant type *Pf*DHFR came from the steric clash with Asn108 mutation. Our particular interaction energy studies can verify this evidence with the obtained repulsive energy.

Conclusion

The CoMFA analysis is a very powerful method for ligand-based drug design. This method has been successful in designing new potent inhibitors for many drugs. Therefore, in this study, the CoMFA method was selected to build a linear equation of the quantitative structure activity relationship of the pyr derivatives that are active against quadruple mutant type *Pf*DHFR. The combined C_{sp3} (+1), O_{sp3} (−1) and H (+1) probe atoms model was selected to represent the CoMFA moelcular fields for accounting the different types of interactions between mutant *Pf*DHFR binding site and pyr derivatives. The steric contour maps of this model suggest that **X** and **R** substitutions favoured a bulky group which is opposite to **Y** substitution. Electrostatic maps are displayed surrounding the phenyl ring of the **R** substituent of the template compound which means that an electron donating substituent on the phenyl ring will increase the biological activity. Therefore, the characteristics of new design inhibitors are the bulky group on the **X** substitution, the hydrogen atom on the **Y** substitution and the long chain on the **R** substitution. Moreover, we also performed MP2/6-31G(d,p) quantum chemical calculations with BSSE-CP energy correction to investigate the particular interaction energy of compounds **1** (pyr) and **6** (Cl substituent

Table IV. Particular interaction energy (kcal/mol) of **1** (pyr) and **6** with individual residues, calculated at MP2/6-31G(d,p) and MP2/6-31G(d,p) levels with BSSE-CP.

	Particular interaction energy (kcal/mol)			
	Compound **1**		Compound **6**	
Amino Acids	MP2/6-31G(d,p)	MP2/6-31G(d,p) with BSSE-CP	MP2/6-31G(d,p)	MP2/6-31G(d,p) with BSSE-CP
Ile14	− 8.034	− 4.172	− 8.735	− 4.298
Cys15	− 4.654	− 1.203	− 4.737	− 1.272
Ala16	− 2.122	− 0.667	− 2.194	− 0.506
Val45	− 0.183	− 0.183	0.002	0.002
Leu46	− 0.096	1.223	− 1.517	− 0.878
Trp48	− 0.535	− 0.526	− 0.554	− 0.548
Cys50	− 0.063	− 0.063	− 0.025	− 0.025
Ile51	0.044	0.044	0.056	0.056
Asp54	− 17.159	− 10.139	− 17.251	− 10.250
Met55	0.191	1.856	0.303	1.933
Tyr57	− 0.489	− 0.317	− 0.343	− 0.226
Phe58	− 9.634	− 3.884	− 9.511	− 3.326
Arg59	− 1.476	− 1.475	− 1.744	− 1.743
Asn108	1.173	3.839	− 3.355	− 0.895
Ser111	0.085	1.862	− 0.921	− 0.758
Ile112	0.239	1.790	1.517	3.237
Pro113	− 0.118	− 0.114	0.038	0.038
Phe116	− 0.085	− 0.085	0.052	0.052
Leu119	− 0.233	− 0.219	− 0.247	0.531
Leu164	− 5.888	− 3.470	− 4.072	− 2.165
Gly165	− 0.062	− 0.022	0.026	0.071
Thr185	− 0.538	0.171	− 0.458	0.202

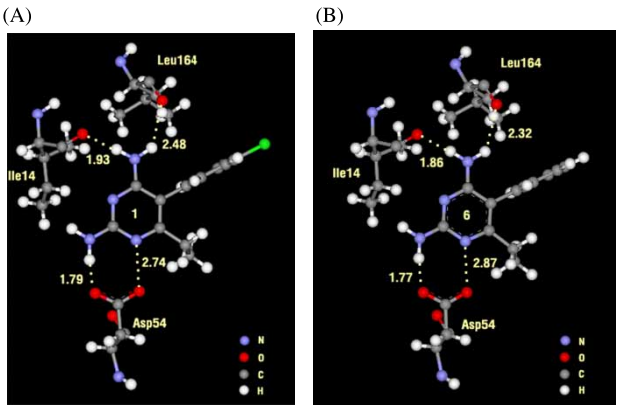

Figure 7. H-bond distances between inhibitor and residues in the binding pocket; (A) compound **1** and (B) compound **6** (in Å).

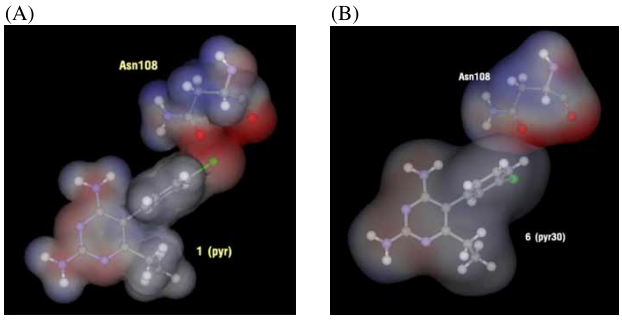

Figure 8. The electrostatic potential is shown on the solvent accessible surface as red for negative and blue for positive values for Asn108 interacted with (A) compound **1** and (B) compound **6**.

on **X**). The obtained results clearly show that Asn108 is the cause of pyr resistance with the highest repulsive interaction energy and negative electrostatic potential. Accordingly, this calculation is consistent with the unfavoured steric region of CoMFA contour maps. The CoMFA and particular interaction energy analyses will be useful for identifying the structural features of potent pyr derivatives active against quadruple mutant type *Pf*DHFR which is an important target of malaria chemotherapy.

Acknowledgements

This work was supported by the Thai Graduate Institute of Science and Technology (TGIST) Funds (TG-22-11-845D) under the National Science and Technology Development Agency, Thailand. S.H. is grateful to the Thailand Research Fund (RSA5080005). The Post-graduate Education and Research Program in Petroleum, Petrochemical Technology and Advanced Materials, Commission on Higher Education (CHE), the Kasetsart University Research and Development Institute (KURDI) and the Graduate School Kasetsart University Scholarship are gratefully acknowledged for financial support. We would like to thank the Large Scale Research Laboratory of the National Electronics and Computer Technology (NECTEC), National Center for Genetic Engineering and Biotechnology (BIOTEC), LCAC and the computing center of KU for research facilities. This work has partially been supported by the National Nanotechnology Center (NANOTEC), NSTDA, Ministry of Science and Technology, Thailand, through its program of Center of Excellence Network. Medicines for Malaria Venture (MMV), Wellcome Trust, and UNICEF/UNDP/World Bank/-WHO Special Programme for Research and Training in Tropical Diseases (TDR) for YY and SK. SK is an international scholar of Howard Hughes Medical institute (HHMI, USA).

Declaration of interest: The authors report no conflicts of interest. The authors alone are responsible for the content and writing of the paper.

References

[1] Snow RW, Guerra CA, Noor AM, Myint HY, Hay SI. Estimating clinical episodes of malaria. Nature 2005;434: 214–217.

[2] Prapunwattana P, Sirawaraporn W, Yuthavong Y, Santi DV. Chemical synthesis of the *Plasmodium falciparum* dihydrofolate reductase-thymidylate synthase gene. Mol Biochem Parasitol 1996;83:93–106.

[3] Yuvaniyama J, Chitnumsub P, Kamchonwongpaisan S, Vanichtanankul J, Sirawaraporn W, Taylor P, Walkinshaw MD, Yuthavong Y. Insights into antifolate resistance from malarial DHFR-TS structures. Nat Struct Biol 2003;10:357–365.

[4] Dasgupta T, Anderson KS. Probing the role of parasite-specific, distant structural regions on communication and catalysis in the bifunctional thymidylate synthase- dihydrofolate reductase from *Plasmodium falciparum*. Biochemistry 2008;47(5):1336–1345.

[5] Delfino RT, Santos-Filho OA, Figueroa-Villar JD. Type2 antifolates in the chemotherapy of *falciparum* malaria. J Braz Chem Soc 2002;13:727–741.

[6] Marbiah NT, Petersen E, David K, Magbity E, Lines J, Bradley DJ. A controlled trial of lambda-cyhalothrin-impregnated bed nets and/or dapsone/pyrimethamine for malaria control in Sierra Leone. Am J Trop Med Hyg 1998;58(1):1–6.

[7] Sowunmi A, Fateye BA, Adedeji AA, Gbotosho GO, Happi TC, Bamgboye AE, Bolaji OM, Oduola AMJ. Predictors of the failure of treatment with pyrimethamine-sulfadoxine in children with uncomplicated *falciparum* malaria. Acta Trop 2006;98:6–14.

[8] Alker AP, Mwapasa V, Meshnick R. Rapid real-time PCR genotyping of mutations associated with sulfadoxine-pyrimethamine resistance in *Plasmodium falciparum*. Antimicrob Agents Chemother 2004;48(8):2924–2929.

[9] Warhurst DC. Resistance to antifolate in *Plasmodium falciparum*, the causative agent of tropical malaria. Sci Prog 2002;85:89–111.

[10] Sirawaraporn W. Dihydrofolate reductase and antifolate resistance in malaria. Drug Resist Updat 1998;1:397–406.

[11] Delfino RT, Santos-Filho OA, Figueroa-Villar JD. Molecular modeling of wild-type and antifolate resistant mutant *Plasmodium falciparum* DHFR. Biophys Chem 2002;98: 287–300.

[12] Peterson DS, Milhous WK, Wellems TE. Molecular basis of differential resistance to cycloguanil and pyrimethamine in *Plasmodium falciparum* malaria. Proc Natl Acad Sci USA 1990; 87:3018–3022.

[13] Sirawaraporn W, Sathitkul T, Sirawaraporn R, Yuthavong Y, Santi DV. Antifolate-resistant mutants of *Plasmodium falciparum* dihydrofolate reductase. Proc Natl Acad Sci USA 1997; 94:1124–1129.

[14] Hastings IM, Donnelly MJ. The impact of antimalarial drug resistance mutations on parasite fitness, and its implications for the evolution of resistance. Drug Resist Updat 2005;8: 43–50.

[15] Walliker D, Hunt P, Babiker H. Fitness of drug-resistant malaria parasites. Acta Trop 2005;94:251–259.

[16] Kamchonwongpaisan S, Quarrell R, Charoensetakul N, Ponsinet R, Vilaivan T, Vanichtanankul J, Tarnchompoo B, Sirawaraporn W, Lowe G, Yuthavong Y. Inhibitors of multiple mutants of *Plasmodium falciparum* dihydrofolate reductase and their antimalarial activities. J Med Chem 2004;47:673–680.

[17] Kubinyi H, Kubinyi H. QSAR: Hansch Analysis and Related Approaches *VCH: Weinheim*. 1993.

[18] Hansch C, Leo A. Exploring QSAR. Fundamentals and Applications in Chemistry and Biology. Washington, DC: American Chemical Society; 1995.

[19] Cramer RD, III, Patterson DE, Bunce JD. Comparative molecular field analysis CoMFA: 1. Effect of shape on binding of steroids to carrier proteins. J Am Chem Soc 1988;110: 5959–5967.

[20] Kubinyi H, Flokers G, Martin YC. 3D QSAR in drug design: Ligand-protein interactions and molecular similarlity. Perspect Drug Discovery Des 1998;:3–398.

[21] Sao SS, Karplus M. Evaluation of designed ligands by a multiple screening method: Application to glycogen phosphorylase inhibitors constructed with a variety of approaches. J Comput Aided Mol. Des 2001;15:613–647.

[22] Saen-oon S, Kuno M, Hannongbua S. Binding energy analysis for wild-type and Y181C Mutant HIV-1 RT/8-Cl TIBO complex structures: Quantum chemical calculations based on the ONIOM method. PROTEINS: Structure, Function, and Bioinformatics 2005;61:859–869.

[23] Kuno M, Hongkrengkai R, Hannongbua S. ONIOM-BSSE scheme for H–¶ system and applications on HIV-1 reverse transcriptase. Chem Phys Lett 2006;424:172–177.

[24] SYBYL 7.0., Tripos Associates Inc., 1699 South Hanley Road, Suite 303, St. Louis, Missouri 63144, USA.

[25] Streitwieser A. Molecular Orbital Theory for Organic Chemists. Wiley: New York; 1961.

[26] Clark M, Cramer RD, III. The probability of chance correlation using partial least squares (PLS). Quant Struct-Act Relat 1993;12(2):137–145.

[27] Bush BL, Nachbar RB, Jr. Sample-distance partial least squares: PLS optimized for many variables, with application to CoMFA. J Comput Aided Mol Des 1993;7:587–619.

[28] Cho SJ, Tropsha A. Cross-validated R2-guided region selection for comparative molecular field analysis: A simple method to achieve consistent results. J Med Chem 1995;38: 1060–1066.

[29] Golbraikh A, Tropsha A. Beware of q2!. J Mol Graph Mod 2002;20:269–276.

[30] Hannongbua S, Nivesanond K, Lawtrakul L, Pungpo P, Wolschann P. 3D-quantitative structure-activity relationships of HEPT derivatives as HIV-1 reverse transcriptase inhibitors, based on *ab initio* calculations. J Chem Inf Comput Sci 2001; 41:848–855.

[31] Frisch MJ, Trucks GW, Schlegel HB, Scuseria GE, Robb MA, Cheeseman JR, Montgomery JA, Jr., Vreven T, Kudin KN, Burant JC, Millam JM, Iyengar SS, Tomasi J, Barone V, Mennucci B, Cossi M, Scalmani G, Rega N, Petersson GA, Nakatsuji H, Hada M, Ehara M, Toyota K, Fukuda R, Hasegawa J, Ishida M, Nakajima T, Honda Y, Kitao O, Nakai H, Klene M, Li X, Knox JE, Hratchian HP, Cross JB, Adamo C, Jaramillo J, Gomperts R, Stratmann RE, Yazyev O, Austin AJ, Cammi R, Pomelli C, Ochterski JW, Ayala PY, Morokuma K, Voth GA, Salvador P, Dannenberg JJ, Zakrzewski VG, Dapprich S, Daniels AD, Strain MC, Farkas O, Malick DK, Rabuck AD, Raghavachari K, Foresman JB, Ortiz JV, Cui Q, Baboul AG, Clifford S, Cioslowski J, Stefanov BB, Liu G, Liashenko A, Piskorz P, Komaromi I, Martin RL, Fox DJ, Keith T, Al-Laham MA, Peng CY, Nanayakkara A, Challacombe M, Gill PMW, Johnson B, Chen W, Wong MW, Gonzalez C, Pople JA. *Gaussian 03*, revision B.05; Gaussian, Inc.: Pittsburgh: 2003.

[32] Boys SF, Bernardi F. The calculations of small molecular interaction by the difference of separate total energies some procedures with reduced error. Mol Phys 1970;19:553–566.

[33] Yuthavong Y. Basis for antifolate action and resistance in malaria. Microb Inf 2002;4:175–182.

[34] Rastelli G, Sirawaraporn W, Sompornpisut P, Vilaivan T, Kamchonwongpaisan S, Quarrell R, Lowe G, Thebtaranonth Y, Yuthavong Y. Interaction of pyrimethamine, cycloguanil, WR99210 and their Analogues with *Plasmodium falciparum* Dihydrofolate reductase: Structural basis of antifolate resistance. Bioorg Med Chem 2000;8:1117–1128.

[35] Yuthavong Y, Yuvaniyama J, Chitnumsub P, Vanichtanankul J, Chusacultanachai S, Tarnchompoo B, Vilaivan T, Kamchonwongpaisan S. Malarial (*Plasmodium falciparum*) dihydrofolate reductase-thymidylate synthase: Structural basis for antifolate resistance and development of effective inhibitors. Parasitology 2005;130:249–259.